

MAGNETIC PHASE TRANSITIONS
IN RARE-EARTH-RICH GLASSES

by

KWAN MYUNG LEE

B.S., Busan National University, KOREA, 1982

A MASTER'S THESIS

Submitted in partial fulfillment of the
requirements for the degree

MASTER OF SCIENCE

Department of Physics

KANSAS STATE UNIVERSITY

Manhattan, Kansas

1987

Approved by:

Michael J. O'Keefe
Major Professor

LU
2.0.00
.T4
PHYS
1987
L43
C. 2

ACKNOWLEDGEMENTS

ALL207 308963

I thank Jesus Christ for giving me an ability to finish this work.

I would like to thank my father and mother for their love.

I would like to thank Young-Ae Kim for her love and encouragement.

I would like to thank my major professor, Dr. M.J. O'Shea, for his guidance and help throughout the course of this work.

I would like to thank Seung-Ae Park for her help to draw figures.

I would like to thank Wan-Soo Kim and Seung-Mok Lee for their help to type and print this thesis.

I would like to thank my Korean friends for their help and friendship.

I thank Dr. D.J. Sellmyer at University of Nebraska at Lincoln for the use of the splat-cooling apparatus.

I thank Dr. G. Hadjipanayis for his providing us liquid Helium and letting us use some of his apparatus.

I thank Dr. D. Dragsdorf for the use of x-ray apparatus.

To the faculty and staff of the Physics Department, and my fellow graduate students, I thank them for their help and encouragement.

TABLE OF CONTENTS

Chapter	Page
1 INTRODUCTION AND PREVIOUS WORK	1
2 THEORETICAL ASPECTS	5
2.1 Microscopic Interactions in Rare-Earth-Rich Glasses	5
2.1.1 Exchange Interactions	5
2.1.2 Random Magnetic Anisotropy (RMA) Interactions	7
2.2 Magnetic States in Exchange Fluctuation and RMA Systems	8
3 EXPERIMENTAL METHODS	13
3.1 Sample Preparation	13
3.1.1 Alloy Preparation	13
3.1.2 Preparing the Metallic Glass	15
3.2 Sample Characterization by X-ray Diffraction ..	15
3.3 Measurement technique	16
3.3.1 AC Susceptibility	16
3.3.2 Vibrating Sample Magnetometer (VSM) ...	20
4 MAGNETIC TRANSITIONS IN Gd ₆₅ Co ₃₅ -BASED ALLOYS	22
4.1 Magnetic Phase Transition in Gd ₆₅ Co ₃₅	22
4.2 Magnetic Phase Transition in Gd _{65-x} R _x Co ₃₅	22
4.2.1 R = La, Ce	24
4.2.2 R = Pr, Nd, Sm, Tb, Dy, Ho	26
5 DOUBLE-TRANSITION BEHAVIOR IN THE Er SYSTEM	34
5.1 Magnetic Phase Transitions in the Er System ..	34
5.1.1 In-Phase Susceptibility, χ'	34

Chapter	Page
5.1.2	Out-of-Phase Susceptibility, χ'' 37
5.1.3	The Field-Cooled Magnetization 37
5.2	Further Studies on the Double-Transition Behavior in the Er System 39
5.2.1	Variation of the Alloy Components 39
5.2.2	Samples Made by Melt-Spinning Technique 39
5.3	Explanation of the Double-Transition Behavior 41
5.3.1	Calculation of RMA Strength D 41
5.3.2	The Double-Transition Behavior for Small Enough RMA 43
5.3.3	Comparison with Exchange Fluctuation Systems 43
6	SCALING AT THE SPERMAGNETIC TRANSITION 47
6.1	Linear Scaling 48
6.2	Non-linear Scaling 49
6.3	Discussions 53
7	SUMMARY AND CONCLUSIONS 57
	REFERENCES 59
	ABSTRACT TITLE
	ABSTRACT

LIST OF FIGURES

Figure	Page
<p>1.1 Possible magnetic structures in metallic glasses. In the SM and SG states the spins are frozen in random directions. The ferrimagnetic state only exists in two component systems (since two unequal moments are required).....</p>	3
<p>2.1 (a) The direct exchange interaction as a function of ion separation r_{ij}. The scale of r_{ij} depends on the extent of the d electron wave function.</p> <p>(b) The RKKY exchange interaction as a function of ion separation r_{ij}. k_F is the Fermi wave vector.....</p>	6
<p>2.2 (a) Magnetic phases in mean field theory of a Heisenberg exchange fluctuation system.</p> <p>(b) Schematic phase diagram of a real system with exchange fluctuations.....</p>	9
<p>2.3 (a) Magnetic phases in mean field theory of a RMA system.</p> <p>(b) Schematic phase diagram of a real system with RMA.</p> <p>(c) Magnetic phases in correlation function calculation of a RMA system.....</p>	11
<p>3.1 Schematic of arc furnace and splat-cooling apparatus.....</p>	14

Figure	Page
3.2 X-ray diffractograms for (a) the Permaquartz, (b) $Gd_{65}Co_{35}$ and (c) $Tb_{65}Co_{35}$. The scanning time was 0.4°/min in each case.....	17
3.3 Schematic of VSM and ac susceptibility apparatus...	18
4.1 (a) AC susceptibility as a function of temperature and (b) hysteresis loops at 4.2 K for the $Gd_{65-x}La_xCo_{35}$ system.....	23
4.2 (a) AC susceptibility as a function of temperature and (b) hysteresis loops at 4.2 K for the $Gd_{65-x}Ce_xCo_{35}$ system.....	25
4.3 Magnetic phase diagram for R = La, Ce, Pr, Nd, Tb, Dy and Ho systems.....	27
4.4 AC susceptibility for $Gd_{65-x}Tb_xCo_{35}$. The lower panel shows the in-phase part (χ') and the upper panel shows the out-of-phase part (χ''). The χ'' curves are shifted with respect to each other for clarity.....	28
4.5 AC susceptibility for (a) Pr, (b) Nd, (c) Dy and (d) Ho systems.....	29
4.6 Hysteresis loops for selected samples of (a) Tb and (b) Dy systems at 4.2 K.....	31
4.7 (a) Coercivity H_C and (b) saturation magnetization M_0 as a function of composition x for R = La, Ce, Pr, Nd, Sm, Tb, Dy, Er and Ho systems.....	33
5.1 AC susceptibility for $Gd_{65-x}Er_xCo_{35}$. The lower panel shows the in-phase part (χ') and the upper	

Figure	Page
panel shows the out-of-phase part (χ'').....	35
5.2 Magnetic phase diagram for the Er system.....	36
5.3 Field cooled magnetization for some selected Er alloys.....	38
5.4 AC susceptibility for (a) $Gd_{65-x}Er_xNi_{35}$ and (b) $(Gd_{65-x}Er_xCo_{35})_{90}B_{10}$	40
5.5 Hysteresis loops at 4.2 K in the Er system.....	46
6.1 Scaling of the magnetic isotherms for the $x = 50$ at. % Tb alloy plotted in (a) linear and (b) logarithmic form. The temperatures of the magnetic isotherms are $(T)T_C$: 111.3 (+), 109.8 (\diamond), 108.4 (o), 106.8 (Δ), 105.4 (\square), $(T)T_C$: 104.1 (+), 102.4 (\diamond), 101.0 (o), 99.7 (Δ), 98.5 (\square).....	50
6.2 Deviations from linear scaling below about 1 kOe...	51
6.3 Non-linear scaling of the magnetic isotherms for the $x = 50$ at. % Tb alloy plotted in logarithmic form. The temperatures of the magnetic isotherms are $(T)T_C$: 108.5 (\square), 107.5 (Δ), 106.4 (o), 105.3 (\diamond), $(T)T_C$: 104.3 (\square), 103.2 (Δ), 101.8 (o), 100.5 (\diamond).....	54

LIST OF TABLES

Table		Page
5.1	Values of the anisotropy and transition temperatures T_A and T_C (see text) along with the resulting D/I_0 ratio for some selected Er and Tb alloys. The estimated errors for T_A and T_C are 15 % and 0.5 % respectively.....	42
6.1	Non-linear exponents in SG and SM systems.....	55

CHAPTER 1

INTRODUCTION AND PREVIOUS WORK

Study of the magnetic properties of amorphous metallic alloys began in 1960 when Gubanov showed theoretically that ferromagnetism (FM) can exist in amorphous systems [1]. Amorphous systems differ from crystalline systems in that they do not have long-range structural order. In the literature the terms "amorphous" and "glassy" are often used interchangeably. In this work we shall refer to rare-earth-transition metal alloys as metallic glasses.

In this introduction we shall give an overview of the work discussed in this thesis. About a decade ago, Rhyne et al. [2] showed that both the curie temperature T_C and the spontaneous magnetization $M(T)$ of metallic glasses containing anisotropic rare-earths are substantially lower than those of the corresponding crystalline Laves phase alloys. Random magnetic anisotropy (RMA) exists in the metallic glasses due to the presence of anisotropic rare-earths. In order to explain the magnetic properties of such systems, Harris, Plischke and Zuckermann [3] introduced a Hamiltonian consisting of two terms, a Heisenberg exchange and a random magnetic anisotropy (RMA) :

$$H = - I_0 \sum_{i,j} (\vec{S}_i \cdot \vec{S}_j) - D \sum_i (\hat{n}_i \cdot \vec{S}_i)^2 . \quad (1.1)$$

I_0 is the strength of the average exchange interaction, \vec{S} is the electron spin and \hat{n}_i is a unit vector which denotes the

direction of the local anisotropy strength, D_i , at site i and varies at random in direction from site to site. Rare-earth-rich metallic glasses show a wide range of magnetic behavior ranging from ferromagnetism (FM) to speromagnetism (SM) due to the presence of RMA. In the SM state the spins are frozen in random directions due to the RMA. This state is similar to the spin-glass (SG) state where RMA is not present and the freezing is due to competing ferromagnetic and anti-ferromagnetic interactions. The SM, SG and a number of other magnetic states found in amorphous systems are shown schematically in Fig. 1.1.

In this thesis we will present studies of rare-earth metallic glasses and compare experimental results with some recent theoretical predictions. The glasses studied here have composition $Gd_{65-x}R_xCo_{35}$ (composition in atomic percent), where R denotes a rare-earth. Othman studied the above system for $R = Ce, Pr, Nd, Tb, Dy, Er$ with $0 \leq x \leq 30$ using ac susceptibility [4]. Here we extend the composition x to 65 at. %, include the rare-earth elements La, Sm, Ho and in addition we study the magnetization behavior.

RMA is induced in a controlled fashion in $Gd_{65}Co_{35}$ by alloying with anisotropic rare-earths. Othman [4] showed that alloying with Er produces a paramagnetic (PM) to ferromagnetic (FM) to speromagnetism (SM) sequence of transitions with decreasing temperature for small enough Er content. We have studied this system further and we will

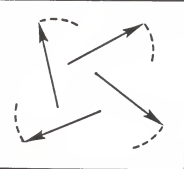
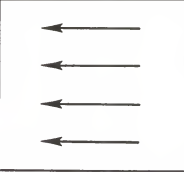
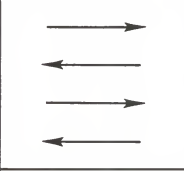
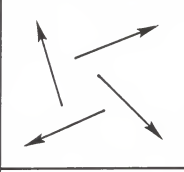
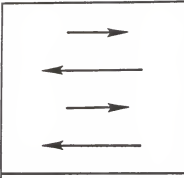
	PM				
	FM				
	Anti-FM				
	SM or SG				
	Ferri-magnet				

Fig. 1.1 Possible magnetic structures in metallic glasses.

In the SM and SG states the spins are frozen in random directions. The ferrimagnetic state only exists in two component systems (since two unequal moments are required).

argue that this behavior is due to the small RMA induced by the Er. In all the other anisotropic rare-earth glasses studied the RMA is found to be stronger and a smooth cross-over from PM-FM to PM-SM behavior is found with increasing anisotropic rare-earth content.

Othman [4] studied the scaling behavior of non-linear susceptibility via ac susceptibility for selected Tb samples to determine whether the SM transition is a true phase transition. A good scaling of the isotherms was not obtained in the work. Here we improve the scaling analysis for the $x = 50$ Tb sample by measuring non-linear magnetization in a vibrating sample magnetometer (VSM) where higher fields and better temperature control than in ac susceptibility are possible and we show that a scaling of the isotherms does indeed occur as expected for a phase transition.

CHAPTER 2

THEORETICAL ASPECTS

2.1 Microscopic Interactions in Rare-Earth-Rich Glasses

To describe the magnetic properties of metallic glasses based on the rare earths, we need to understand two types of interactions; exchange interactions and RMA interactions. In this chapter we will discuss these interactions and also models incorporating them.

2.1.1 Exchange Interactions

Exchange interactions in metallic glasses are either direct exchange or indirect RKKY (Ruderman, Kittel, Kasuya and Yosida) [5] exchange. The direct exchange interaction exists in the transition metal alloys where 3d-shells overlap. It is essentially a nearest neighbour interaction. In rare-earth rich metallic glasses the magnetic 4f shells are well localized and so do not overlap, the direct exchange interaction is negligible and the RKKY interaction is important. The strength of the exchange is a function of ion separation r_{ij} for both of these exchange interactions and is shown schematically for direct and RKKY exchange in Fig. 2.1. The exchange interaction strength in the case of the RKKY interaction depends on $S(S+1)$. In amorphous alloys there is a range of interatomic spacings r_{ij} and the result is fluctuations in exchange strength. In some cases the fluctuations are so strong that both ferromagnetic (positive

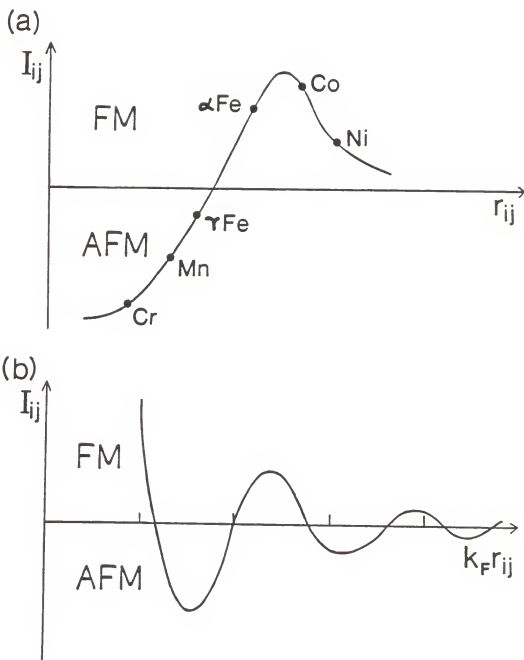


Fig. 2.1 (a) The direct exchange interaction as a function of ion separation r_{ij} . The scale of r_{ij} depends on the extent of the d electron wave function. (b) The RKKY exchange interaction as a function of ion separation r_{ij} . k_F is the Fermi wave vector.

1) and antiferromagnetic (negative I) interactions are present. As a result a magnetic ion can receive contradictory exchange information from its neighbors depending on their distance leading to frustration in the microscopic interactions. An interesting consequence is the occurrence of the spin-glass (SG) phase at sufficiently low temperatures.

The simplest model Hamiltonian incorporating exchange fluctuations is

$$H = - \sum_{ij} (I_0 + \Delta I_{ij}) \vec{S}_i \cdot \vec{S}_j \quad (2.1)$$

I_0 is an average ferromagnetic exchange, ΔI_{ij} represents the exchange fluctuations about the mean I_0 , $\langle ij \rangle$ denotes a pair of spin sites and \vec{S}_i is a spin vector localized at site i . In real rare-earth-transition metal alloys the total exchange will be some combination of direct and RKKY exchange.

2.1.2 Random Magnetic Anisotropy (RMA) Interactions.

Metallic glasses containing non s-state rare-earth ions show very hard magnetic characteristics, such as large low temperature coercivities and an extremely slow approach to saturation. Also, around the coercive field sharp magnetization jumps are sometimes observed at low enough temperatures. In an attempt to explain these characteristics, Harris, Plischke and Zuckermann (HPZ) [3] have proposed a model involving RMA. The Hamiltonian for this model is given

by Eq. (1.1).

The origin of the strong RMA in rare-earth glasses lies in the strong random electric field gradients present in these alloys. These electric field gradients are the amorphous analogue of the crystal fields responsible for the huge magnetocrystalline anisotropy in crystalline anisotropic (non-zero orbital angular momentum) rare-earth alloys [5]. Spin-orbit coupling is required and so RMA is not important in transition metal (TM) metallic glasses where the orbital part of the angular momentum is quenched. RMA comes about when the anisotropic charge of a rare-earth ion responds to the electric field gradients leading to an easy direction for the total moment of the ion. This easy direction varies at random from site to site because of the random nature of the electric field gradients. Harris et al. [3] first proposed that the RMA in amorphous non s-state rare-earth-rich alloys may be of uniaxial form, i.e., $-D(\hat{n}_i \cdot \vec{S}_i)^2$ ($D > 0$), with the local easy axis of magnetic anisotropy \hat{n}_i , varying from site to site.

2.2 Magnetic States in Exchange Fluctuation and RMA Systems

The model Hamiltonian (Eq. 2.1) has been studied by a number of workers. The phase diagram calculated within mean field theory for Heisenberg spins [7,8] is shown in Fig. 2.2a ($\Delta I = \sqrt{\langle \Delta I_{ij}^2 \rangle}$) along with a schematic diagram of the magnetic phases (shown in Fig. 2.2b) found in real alloys

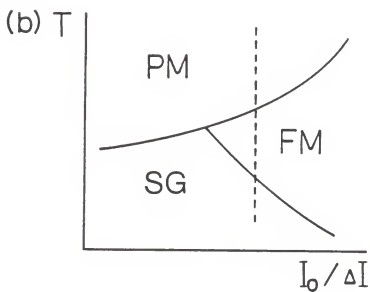
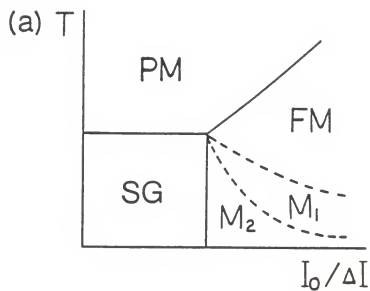


Fig. 2.2 (a) Magnetic phases in mean field theory of a Heisenberg exchange fluctuation system.
 (b) Schematic phase diagram of a real system with exchange fluctuations.

where exchange fluctuations are important [9,10]. The model phase diagram has PM, FM and SG regions and also regions M_1 , M_2 which corresponding to varying degrees of freezing of the transverse component of the spins but no freezing of the longitudinal component so that the phase remains FM. The phase transition behavior of this model (all lines represent continuous phase transitions) is correct only for dimensionality $d \geq 4$ because of the mean field assumption. Computer simulations with $I_0 = 0$ suggest that a PM-SG phase transition still occurs for $d = 3$ [11] for Ising spins. No phase transition is present for Heisenberg spins unless anisotropy is included indicating the importance of anisotropy in real systems (which are made up of Heisenberg spins). None of these simulations reproduce the double-transition behavior (PM-FM-SG transitions) found in real systems, dashed line in Fig. 2.2b. The PM-FM, FM-SG and PM-SG transitions have all been studied experimentally. The experimental scaling behavior at these transitions in all systems studied is consistent with a continuous phase transition [9]. In the case of the PM-SG transition a non-linear scaling is required and these scaling theories are discussed in Sections 2.3 and 6.2.

The magnetic states in an RMA system within mean field theory are shown in Fig. 2.3a [12] along with a schematic diagram of the behavior found experimentally, Fig. 2.3b [7]. An exchange with strength I_0 was assumed (no exchange fluctuations) and the resulting phase diagram again valid

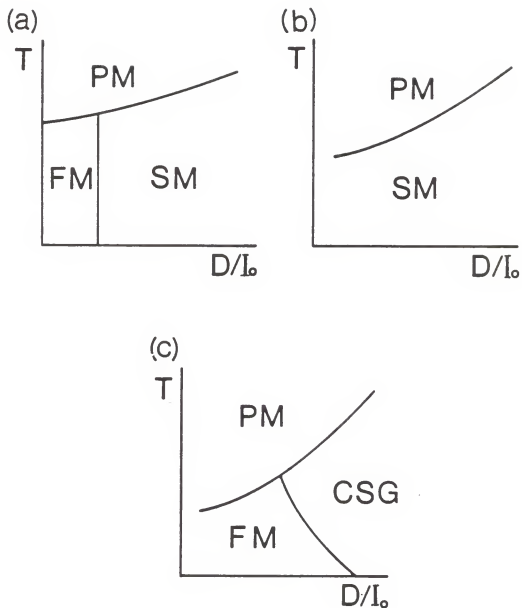


Fig. 2.3 (a) Magnetic phases in mean field theory of a RMA system. (b) Schematic phase diagram of a real system with RMA. (c) Magnetic phases in correlation function calculation of a RMA system.

only for $d \geq 4$ is similar to that for exchange fluctuation systems. This model has not been studied in enough detail to determine whether the phases M_1 , M_2 exist. We shall show in this work that a phase with ferromagnetic character exists for small enough D in real systems so that Fig. 2.3b must be modified.

Some computer simulations of this model for $d = 3$ have been done but none are able yet to answer the question of whether a true phase transition exists at the PM-SG transition in this model. More recently correlation function calculations have been made for $d = 3$ [13] and these indicate a phase diagram, Fig. 2.3c, with PM and SM states and a state called a correlated SG (CSG) state. In this latter state, at short distances the magnetic moments are ferromagnetically correlated but at larger distances the average magnetization vector "wanders" so that the macroscopic moment (or spontaneous magnetization) is zero. No sharp domain walls which delineate regions with different magnetization vector exist in this state as they do in FM materials such as elemental Fe.

CHAPTER 3

EXPERIMENTAL METHODS

3.1 Sample Preparation

The systems studied in this work have the following composition; $Gd_{65-x}R_xCo_{35}$ where R denotes La, Ce, Pr, Nd, Sm, Tb, Dy, Ho, and Er and $x = 0, 2, 4, 10, 20, 30, 40, 50, 65$. All compositions are given in atomic percent.

3.1.1. Alloy Preparation

Elements required to make an alloy are first weighed according to the required composition in the correct stoichiometry. The weighted elements are then combined by melting into a 1 g polycrystalline button. The arc furnace used for this purpose is shown schematically in Fig. 3.1. The elements are placed on a copper anode with smaller chips covered by larger pieces to prevent the smaller ones flying away during melting. The alloy is melted in an arc furnace under an argon-rich atmosphere after pumping and flushing it three times with argon to minimize oxidization during melting. A tungsten electrode with a pointed tip is supplied with current in the range of 10 A to 30 A from a power supply to melt the compound. An arc is produced by moving the tungsten electrode close to the copper anode. The alloy is melted only for a short time to avoid losing mass through evaporation. A homogeneous mixture is insured by moving the arc over the sample and by turning it over and

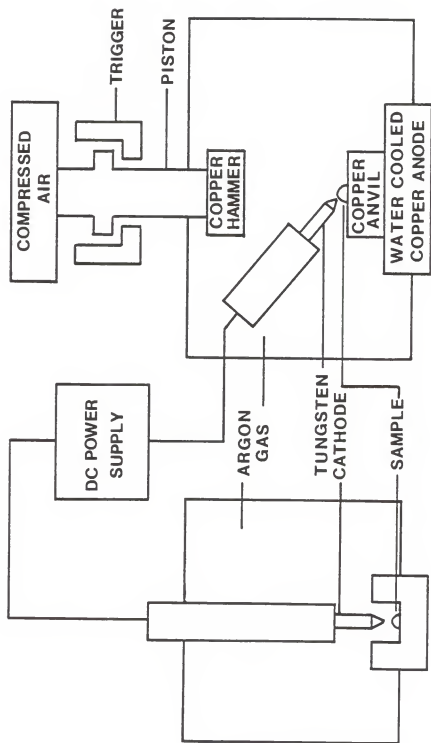


Fig. 3.1 Schematic of arc furnace and splat-cooling apparatus.

remelting. For the alloys discussed here the final buttons have less than 0.1 % mass loss.

3.1.2 Preparing the Metallic Glass

There are a number of techniques used to prepare metallic glasses. A basic requirement for producing the metallic glasses from the melt is very rapid cooling of the alloy with a cooling rate of 10^6 K/s or higher. Most commonly used techniques are the melt-spinning and splat-cooling techniques. The method used in this work is the splat-cooling technique.

Fig. 3.1 shows a schematic of the splat-cooling apparatus. A small portion (0.25 g - 0.3 g) of the original button is placed on the copper anvil. As was done in the arc furnace, the electrode's tip is placed near the copper anode to strike an arc. Current through the electrode required to melt the sample is about 18 A. When the sample is melted, a trigger is released and a hammer driven by high pressure impacts the molten alloy. Just before the impact the air driven hammer knocks the electrode to one side thus removing the arc. The effect of the hammer impact is a very rapid cooling of the sample as heat is conducted away by the copper anvils. The sample obtained is in the form of a circular disc 2-3 cm in diameter and about 50 μ m thick.

3.2 Sample Characterization by X-ray Diffraction

To insure the samples are amorphous, x-ray diffraction measurements were performed. Cu-K α radiation is used as the

x-ray source. Diffracted signals are detected by a proportional counter. A Permaquartz sample was used as a standard and sharp diffracted peaks were observed as illustrated in Fig. 3.2, characteristic of the diffraction pattern of a crystal. In contrast, diffractograms of the samples used in this work showed no evidence of sharp peaks, indicating an amorphous structure. Some microcrystallinity may be present but electron microscopy should be done on the samples to check this. Detailed structural studies of the samples are not the objective of this work. The diffractograms of the amorphous $Gd_{65}Co_{35}$ and $Tb_{65}Co_{35}$ alloys are shown in Fig. 3.2.

3.3 Measurement Technique

3.3.1 AC Susceptibility

AC Susceptibility measurements are made using the apparatus shown schematically in Fig. 3.3. There are two sets of coils which are wound onto a Delrin coil former and placed at the end of a probe. One is a modulation coil which provides an ac field $H_a = H_{0a} \cos \omega t$. The other is a set of pick-up coils which are wound in series opposition and are inside the modulation coil. Without a sample, the signal induced in the upper and lower halves of the pick-up coil cancels out. With a magnetic sample within the lower half of the pick-up coil, the emf's generated become unbalanced and a signal is produced.

The power supply for the modulation coil supplies the

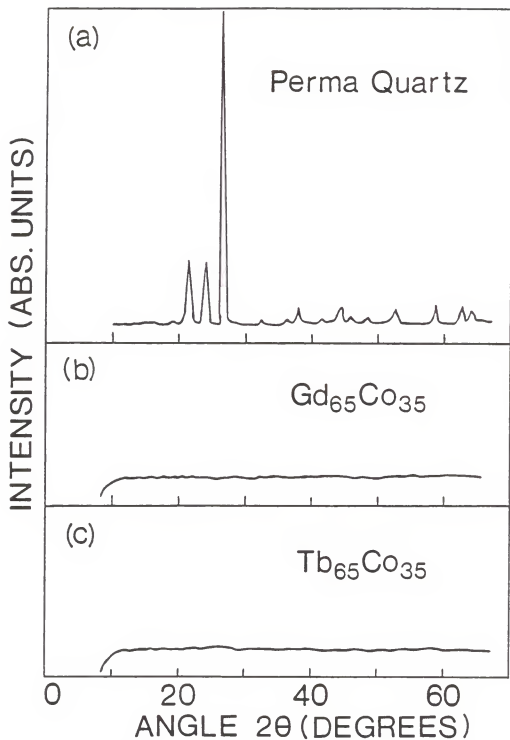


Fig. 3.2 X-ray diffractograms for (a) the Permaquartz, (b) Gd₆₅Co₃₅ and (c) Tb₆₅Co₃₅. The scanning time was 0.4°/min in each case.

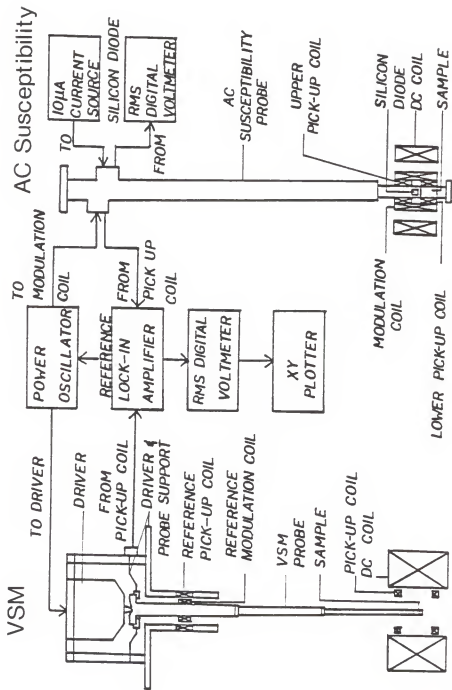


Fig. 3.3 Schematic of VSM and ac susceptibility apparatus.

reference signal for the lock-in amplifier at an audio frequency of about 280 Hz. The amplitude of the measuring field was 1.0 Oe. The signal produced in the pick-up coil is fed back to the lock-in amplifier, converted to a dc signal and amplified. This signal is proportional to the ac susceptibility $\chi_{ac} = dM/dH_a$. The phase of the lock-in amplifier is set to maximize the output signal which is then monitored by a digital voltmeter and plotted on an X-Y plotter. Phase sensitive detection (in the lock-in amplifier) is used to minimize noise. The temperature of the sample is varied by moving the probe up and down in a Helium dewar and measured by a silicon diode placed close to the sample. Temperature conversion from the diode's voltage is provided by the manufacturer (Lakeshore Cryotronics). A 10 μ A current source is used for this diode and its voltage is monitored by a digital voltmeter and plotted on an X-Y plotter.

Rectangular strips about 1 mm by 12 mm are cut from the splat-cooled sample. The strips are placed in a plastic holder in the form of a tube 1 cm long and held in place with GE-7031 varnish (supplied by Lakeshore Cryotronics). The strips are placed with the long axis parallel to the applied ac magnetic field to minimize demagnetization effects. We use about 30 mg's of the strips for this measurement.

The internal susceptibility $\chi_i = dM/dH_i$, where H_i is

the internal field, is obtained by measuring the ac susceptibility χ_{ac} . The internal and applied fields are related by

$$H_i = H_a - NM$$

where N is the geometric demagnetization factor. It should be noted that the demagnetization field is uniform and equal to $-NM$ with $N = 4\pi$ for an ellipsoid. The above equation is only approximate for strips. The internal susceptibility is then given by

$$\chi_i^{-1} = \chi_{ac}^{-1} - N$$

which can be rewritten as

$$\chi_i = \chi_{ac} / (1 - N\chi_{ac}).$$

We consider two limits

- (i) with χ_{ac} small ($\chi_{ac} \ll N$), then $\chi_i \cong \chi_{ac}$
- (ii) with $\chi_{ac} = 1/N$, then $\chi_i \rightarrow \infty$ indicating entry into a ferromagnetic or ferrimagnetic state.

3.2.2 Vibrating Sample Magnetometer (VSM)

A VSM is used to measure the dc magnetization. As shown in Fig. 3.3, a probe driven by a mechanical driver vibrates with a vertical amplitude A and a frequency of 37 Hz. The sample in a constant magnetic field is vibrated up and down in the center of two pick-up coils which are wound in series opposition. Since the sample enters one half of the pick-up coil while leaving the other half, the induced emf's add. The ac output signal is converted to a dc signal which is proportional to magnetization by the lock-in

analyzer, monitored by a digital voltmeter and plotted on an X-Y plotter. The temperature in the sample chamber is lowered by flowing cold helium gas from the liquid helium chamber into the sample chamber via a needle valve. A Si diode is placed near the sample at the end of the VSM probe to monitor the sample's temperature. A heater with a Ga-As diode near it is used to change the temperature of the flowing gas. The temperature of the heater is set by setting the voltage on the Ga-As diode corresponding to the desired temperature for the heater. High field measurements (up to 80 kOe) are made using a superconducting magnet and low field measurements (0-1000 Oe) are made using a wire wound coil.

CHAPTER 4

MAGNETIC TRANSITIONS IN Gd₆₅Co₃₅-BASED ALLOYS

4.1 Magnetic Phase Transition in Gd₆₅Co₃₅

Amorphous Gd₆₅Co₃₅ is a ferrimagnet (see Fig. 1.1) with a Gd spin of 7.5 μ_B /ion and a Co spin of 0.6 μ_B /ion [14]. The ac susceptibility (χ_{ac}) of amorphous Gd₆₅Co₃₅ ($x = 0$) is shown in Fig. 4.1a. The Gd³⁺ ion (Gd is trivalent) has zero angular momentum, so we can neglect RMA effects in this sample. The measured ac susceptibility increases abruptly near $T_c = 184$ K where T_c is the transition temperature defined as the temperature of the peak of χ_{ac} . It reaches the demagnetization limit ($\chi_{ac} = 1/N$) and then shows a small decrease below T_c probably due to the presence of a small amount of anisotropy in Gd₆₅Co₃₅. This sample was used to establish the demagnetization limit calibration for the ac susceptibility apparatus since it was already known to be ferrimagnetic. Other ferro- and ferri-magnetic alloys gave the demagnetization limit within about 3 % of this. The magnetization (M) of Gd₆₅Co₃₅ saturates below 100 Oe as may be seen from Fig. 4.1b because of the lack of anisotropy in this system. Gd₆₅Co₃₅ shows very little hysteresis with a measured coercive field H_c of 10 Oe at 4.2 K for similar reasons.

4.2 Magnetic Phase Transition in Gd_{65-x}R_xCo₃₅

We will discuss the transition behavior observed in

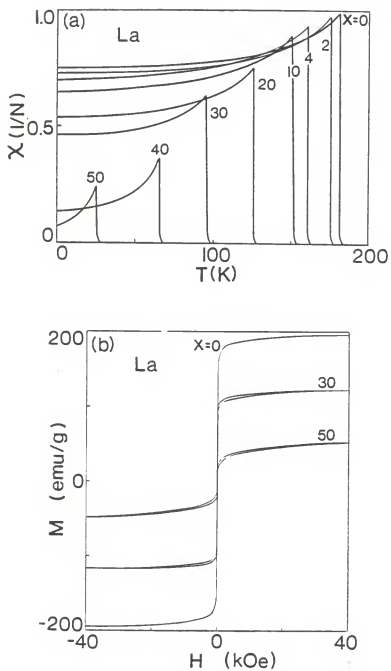


Fig. 4.1 (a) AC susceptibility as a function of temperature and (b) hysteresis loops at 4.2 K for the $Gd_{65-x}La_xCo_{35}$ system.

anisotropic rare-earth-rich glasses as a function of RMA strength D . RMA is induced in a controlled fashion by alloying with the above anisotropic rare-earths. We choose to study anisotropy effects in this system for three reasons. The exchange fluctuations present in this system are not large enough to produce SG behavior since $Gd_{65}Co_{35}$ remains collinearly ordered down to low temperatures. The similarity between Gd and other rare-earth metals allows this system to be alloyed with anisotropic rare-earths while maintaining a homogeneous amorphous structure. Finally the RMA strength may be varied over a significant range by a judicious choice of the rare-earth R and composition x as we show later.

The Er system will be discussed separately in chapter 5 because of its unusual behavior.

4.2.1 $R = La, Ce$

For La^{3+} [15], all the shells are completely filled and the total angular momentum L and spin S of the La ion are zero resulting in a zero net moment. The La ion therefore does not contribute to the magnetization and does not incorporate any significant anisotropy into the system. No increase in coercivity is seen for the La system up to $x = 30$ at. % as shown in Fig. 4.1b.

Similar behavior was seen for the Ce system in Fig. 4.2b implying that it too incorporates no anisotropy. This in turn suggests that Ce is quadrivalent (4+) as has

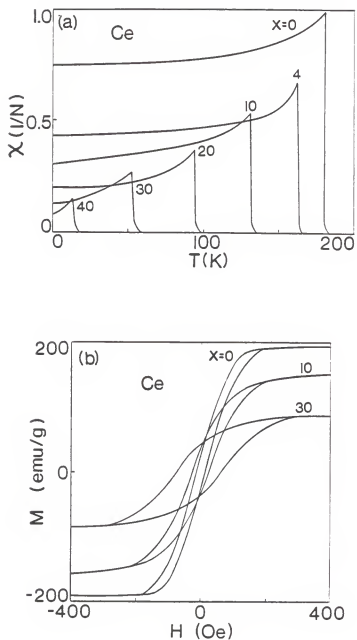


Fig. 4.2 (a) AC susceptibility as a function of temperature and (b) hysteresis loops at 4.2 K for the $Gd_{65-x}Ce_xCo_{35}$ system.

been found for Ce in other alloys by other workers [16]. Although a peak is beginning to develop in the Ce and La systems for larger values of x we do not believe that a SM state is developing since no significant coercivity is found to be present.

AC susceptibilities for La and Ce are shown in Figs. 4.1a and 4.2a respectively. As La or Ce is added, the temperature of the FM transition and the magnitude of the ac susceptibility are smoothly reduced. The transition temperatures as a function of composition x are shown in Fig. 4.3. As can be seen the reduction in ordering temperature is approximately linear with composition x .

4.2.2 R = Pr, Nd, Sm, Tb, Dy, Ho

Fig. 4.4 shows the in-phase (χ') and out-of-phase (χ'') ac susceptibility for R = Tb. AC susceptibilities for R = Pr, Nd, Dy, and Ho are shown in Fig. 4.5a, b, c, and d respectively. These results are similar to the result for the Tb system and we will discuss the Tb system as a standard. Some Sm alloys were also studied (not shown) and the results were also similar to the Tb system. As discussed earlier, the $x = 0$ (Gd₆₅Co₃₅) alloy shows a PM to FM transition. As x increases there is a rapid reduction in peak height of χ' due to the increase of RMA. The fact that the peak heights lie well below the demagnetization limit suggests that they are not in an infinite susceptibility phase. As x is increased in these systems a smooth cross-

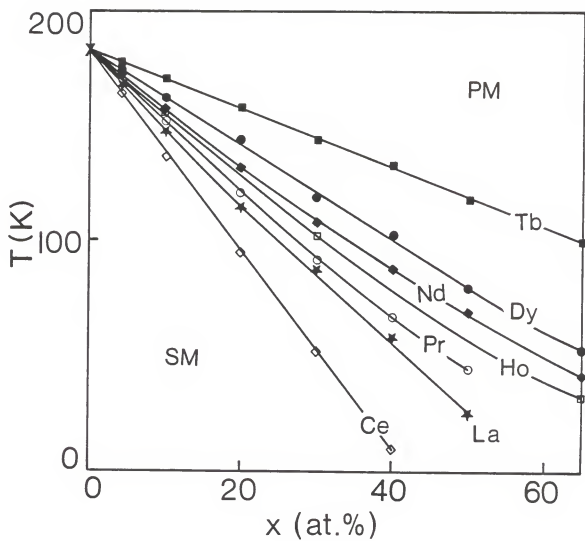


Fig. 4.3 Magnetic phase diagram for $R = \text{La, Ce, Pr, Nd, Tb, Dy, and Ho}$ systems.

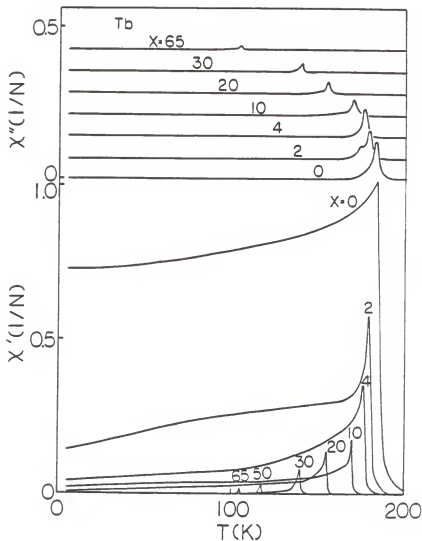


Fig. 4.4 AC susceptibility for $Gd_{65-x}Tb_xCo_{35}$. The lower panel shows the in-phase part (χ') and the upper panel shows the out-of-phase part (χ''). The χ'' curves are shifted with respect to each other for clarity.

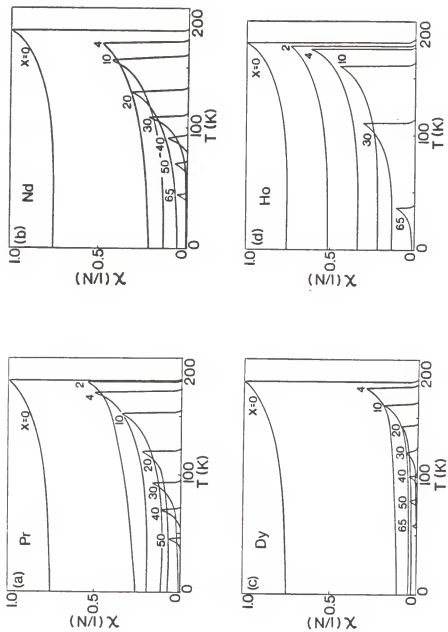


Fig. 4.5 AC susceptibility for (a) Pr, (b) Nd, (c) Dy, and (d) Ho systems.

over from PM-FM to PM-SM behavior is found. The SM transition may also be seen in χ'' which reflects the losses in the system and is shown in the upper panel of Fig. 4.4. The transition temperatures as a function of composition are shown in Fig. 4.3. The ordering temperature decreases as x is increased. This is due in part to a reduction in the average value of $S(S+1)$ as one would expect for a system where the RKKY interaction is being varied. Alloys containing Tb ions which have the highest spin ($S = 3$) have the highest ordering temperature, and La and Ce with the lowest spin ($S = 0$) have the lowest ordering temperature for a given value of x . The ordering temperatures follow in descending order for Tb, Sm, Dy, Nd, Ho, Pr, La and Ce corresponding roughly to descending order of spin magnitude (3, 5/2, 5/2, 3/2, 2, 1, 0 and 0 respectively). The reduction of $S(S+1)$ on alloying with anisotropic rare-earths is not enough by itself to account for the lowering of the ordering temperature. The strength of the RMA also increases with increasing x and we ascribe part of the reduction in transition temperature to increasing RMA strength. Experiments on amorphous and crystalline $Tb_{65}Co_{35}$ [17] have already shown that a strong RMA leads to a lowering of transition temperature. Magnetization measurements up to 80 kOe were used to study hysteresis and Fig. 4.6 shows hysteresis loops for some selected samples of the Tb system.

The coercivity as a function of composition x was

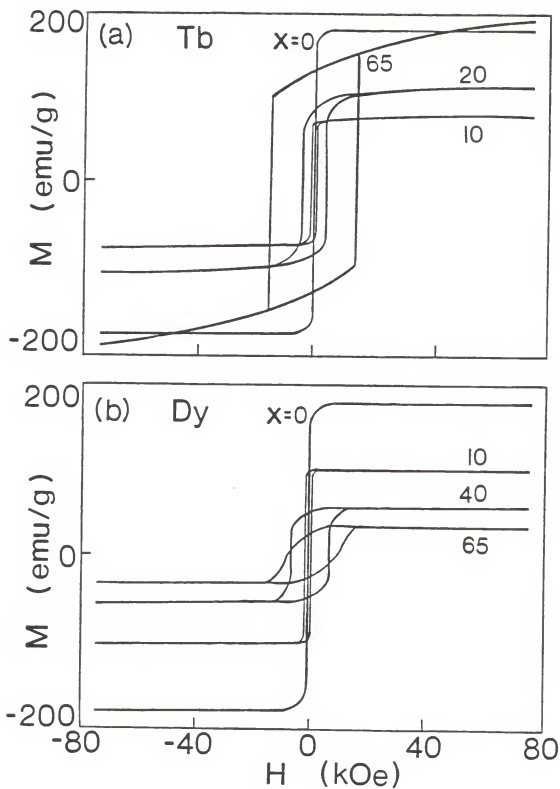


Fig. 4.6 Hysteresis loops for selected samples of (a) Tb and (b) Dy systems at 4.2 K.

determined from magnetization measurements at 4.2 K and these results are shown in Fig. 4.7a. As expected the coercivity increases with increasing Tb content due to the increase in anisotropy strength. Tb appears to induce the largest coercivity for a given value of x of all the rare-earths studied with Dy inducing the second largest value. Fig. 4.7b shows the magnetization M_0 at 80 kOe and 4.2 K as a function of composition x. The magnetization for the Dy system decreases uniformly with x indicating that it is becoming progressively harder to saturate the alloy because of the presence of RMA. Similar behavior was observed for all other anisotropic rare-earths except Tb. As can be seen from Fig. 4.7b the magnetization shows an initial decrease with increasing x but it then turns back up again. We do not understand this behavior but we note that although Tb induced the strongest RMA it also decreases the exchange by the least amount of all the rare-earths studied since it has a spin $S = 3$.

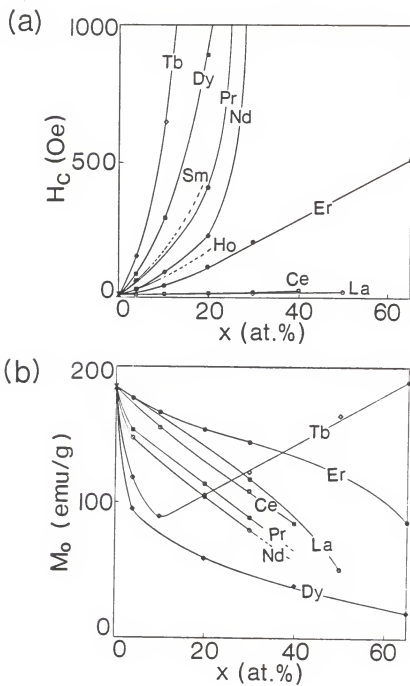


Fig. 4.7 (a) Coercivity H_C and (b) saturation magnetization M_0 as a function of composition x for $R = \text{La, Ce, Pr, Nd, Sm, Tb, Dy, Er, and Ho}$ systems.

CHAPTER 5

DOUBLE-TRANSITION BEHAVIOR IN THE Er SYSTEM

5.1 Magnetic Phase Transitions in the Er System

5.1.1 In-Phase Susceptibility, χ'

Most of the work discussed in this Chapter has been reported in ref. [18]. In all the anisotropic rare-earth glasses discussed above a smooth cross-over from PM-FM to PM-SM behavior is found with increasing anisotropic rare-earth content. But in the Er system we observed double-transition behavior for small enough x .

Fig. 5.1 shows the in-phase (χ') and out-of-phase (χ'') ac susceptibilities for the Er system. As the Er concentration increases the FM transition of the $x = 0$ alloy in χ' shifts linearly to lower temperature and the system crosses over to PM-SM transition behavior for $x \geq 8$ at. % as can be seen from the phase diagram of Fig. 5.2. A lower transition appears in all the Er alloys with $1 < x < 8$ at. % and the in-phase susceptibility remains close to the demagnetization limit in this region. The large susceptibility indicates a phase with ferromagnetic character exists between the upper and lower transition and is probably characterized by short-range ferromagnetic order. There is thus a series of transitions from PM to FM to SM states with decreasing temperature in this composition range. Such double-transition behavior has not been observed previously in alloys containing anisotropic rare-earths. The new transition

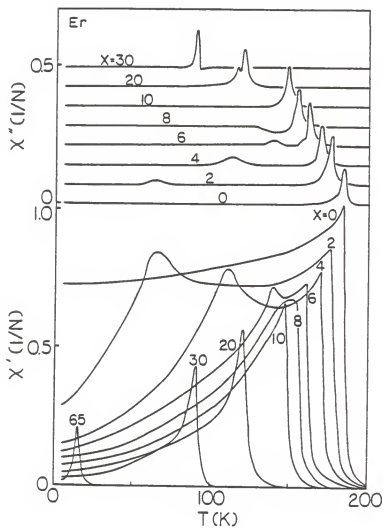


Fig. 5.1 AC susceptibility for $Gd_{65-x}Er_xCo_{35}$. The lower panel shows the in-phase part (χ') and the upper panel shows the out-of-phase part (χ'').

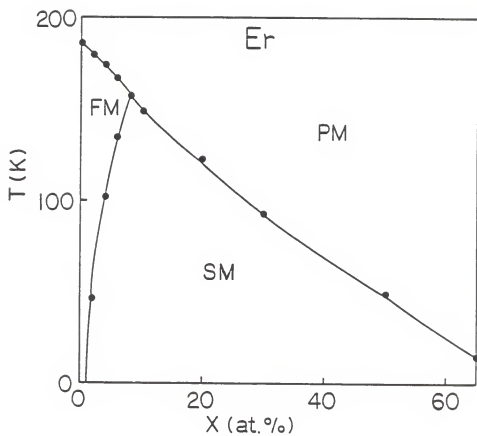


Fig. 5.2 Magnetic phase diagram for the Er system.

moves rapidly to higher temperatures with increasing Er concentration as can be seen from the phase diagram of Fig. 5.2. At about $x = 8$ the double-transition behavior is replaced by a single PM-SM transition.

5.1.2 Out-of-Phase Susceptibility, χ''

Previously the out-of-phase part of the ac susceptibility χ'' , which reflects the losses in the system, has been useful in locating the FM-SG transition [19-21] present in many systems where exchange fluctuations are important. The upper panel of Fig. 5.1 shows χ'' for comparison with χ' and the two peaks in χ'' (corresponding to the PM-FM and FM-SM transitions) for samples with $x < 8$ coincide with the peaks in χ' .

5.1.3 The Field-Cooled Magnetization

The field-cooled magnetization in an applied field of 1.8 Oe is shown in Fig. 5.3 for some selected Er alloys. The earth's field was nulled out during these experiments. An initial rapid rise is observed at the first transition followed by a more gradually increasing magnetization at lower temperatures.

For the Er samples with $x < 8$ at. % a decrease in the field-cooled magnetization is present at a temperature which is close to the lower transition as seen in χ' .

In all the other glass systems discussed above including the Er glasses with $x \geq 8$ at. % no second transition was

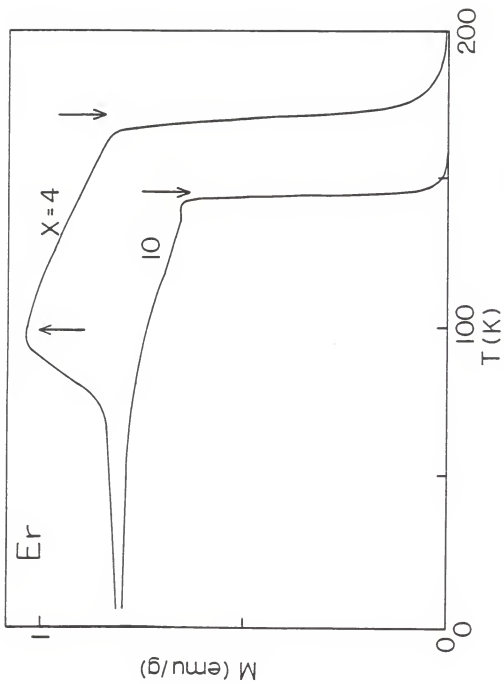


Fig. 5.3 Field cooled magnetization for some selected Er alloys.

seen in the field-cooled magnetization.

5.2 Further Studies on the Double-Transition Behavior in the Er System.

We have done some additional experiments in order to better understand the double-transition behavior in the Er system and we discuss these below.

5.2.1 Variation of the Alloy Components.

We replaced Co₃₅ with Ni₃₅ where Ni is non-magnetic in the R = Er system to see whether there is any change in the double-transition behavior, but similar double-transition behavior was present as shown in Fig. 5.4a. We conclude from this that the double-transition behavior is not related specifically to the ferrimagnetic nature of Gd₆₅Co₃₅.

We also alloyed 10 at. % of boron (B) in some selected Er glasses which would be expected to vary any short-range order present in the glass. We also found similar double-transition behavior as shown in Fig. 5.4b indicating that the double-transition behavior is not likely to be connected with a specific type of short-range order.

5.2.2 Samples Made by Melt-Spinning Technique

We made ribbons for some selected Er alloys by using the melt-spinning technique where any short-range order or microcrystallinity present is likely to be different from the splat-cooled samples. We also observed similar double-transition behavior indicating again that the double-transi-

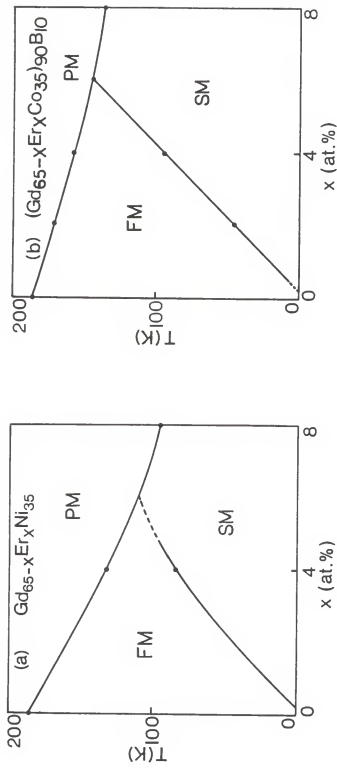


Fig. 5.4 AC susceptibility for (a) $Gd_{65-x}Er_xNi_{35}$ and (b) $(Gd_{65-x}Er_xCo_{35})_{90}Bi_{10}$.

tion behavior is not likely to be connected with a soecific type of short-range order.

5.3 Explanation of the Double-Transition Behavior

RMA is induced in a controlled fashion by alloying with anisotropic rare-earths. We will argue that the double-transition behavior for small enough Er content is due to the small RMA induced by the Er.

5.3.1 Calculation of RMA Strength D.

The introduction of anisotropic rare-earths into Gd-Co glasses induces an RMA and its strength may be measured by using the magnetization-area method. In this method the anisotropy energy per unit volume K is given by [22]

$$K = (3/2) \int_{M_r}^{M_0} M dH$$

where M_0 and M_r are the saturation and remanent magnetization per unit volume respectively. The average anisotropy constant per ion D is given by K/n where n is the number of ions per unit volume and the anisotropy temperature T_A is given by $k_B T_A = D$. The ratio $D/I_0^1 = T_A/T_C$ where T_C is the transition temperature may then be calculated and these quantities are given in Table 5.1. I_0^1 represents the average exchange energy of a spin which is given by $k_B T_C$. As may be seen Er glasses have a small RMA and D/I_0^1 ratio as compared to Tb glasses especially for low concentrations. All the other anisotropic rare-earth glasses studied were found to have D values larger than that of Er for a given

System	x (at. %)	T _A (K)	T _C (K)	D/I ₀ ⁱ
Gd _{65-x} Er _x Co ₃₅	0	0.211	186	0.0011
	10	0.283	149	0.0019
	20	0.879	129	0.0068
	30	1.26	92	0.013
Gd _{65-x} Tb _x Co ₃₅	10	1.31	175	0.0075
	20	2.10	158	0.013
	30	3.01	142	0.021

Table 5.1 Values of the anisotropy and transition temperatures T_A and T_C (see text) along with the resulting D/I₀ⁱ ratio for some selected Er and Tb alloys. The estimated errors for T_A and T_C are 15 % and 0.5 % respectively.

composition x . It should be noted that this method will underestimate D if the alloy is not saturated as in the case of the Tb alloys. The values D/I_0' for the Tb alloys are therefore likely to be larger than those given in Table 5.1. The D/I_0' value for Er is not underestimated since these alloys saturate in low fields (compare Fig. 4.6a with Fig. 5.5).

RMA effects are also present in the coercivity H_C with Er having the smallest value for a given composition of all the anisotropic rare-earths studied as shown in Fig. 4.7a. The $Gd_{65}Co_{35}$ alloy shows a coercivity of about 10 Oe. Hysteresis loops are shown in Fig. 5.5 for some selected Er alloys and Fig. 4.7a shows coercivity as a function of composition x for R = La, Ce, Tb, Dy, Er systems. According to the work of E. Callen et al. [23] the coercivity H_C increases with the anisotropy strength D , but D is proportional to H_C only for large D .

5.3.2 The Double-Transition Behavior for Small Enough RMA

Since Er introduces the smallest RMA of all the anisotropic rare-earths studied as shown above, we associate the double transition behavior with small RMA. If the RMA strength is made too large by either increasing x or alloying with another anisotropic rare-earth, the double-transition behavior is no longer present.

5.3.3 Comparison with Exchange Fluctuation Systems

The double-transition behavior observed in the anisotropic systems of this work is similar to that observed in

exchange fluctuation systems such as the c-AuFe [24], c-EuGdS [19], a-(FeMn)₇₅P₁₆B₆Al₃ [25, 26] and a-(GdLa)₇₂Ga₁₈B₁₀ [20]. It has been known for some time that frustration in the microscopic interactions such as that introduced by exchange fluctuations is a necessary ingredient for spin-glass behavior to be present and this is usually incorporated in model calculations by assuming some distribution of exchange interactions. A small anisotropy is also present in these systems [27] and it was realized recently, mostly through computer simulations, that anisotropy plays a rather fundamental role in stabilizing non-equilibrium spin-glass behavior in Heisenberg systems with short-range interactions. Simulations of the d = 3 exchange fluctuation Heisenberg model [28-30] indicate no spin-glass transition at non-zero temperatures. It is likely that inclusion of anisotropy in this model will produce a non-zero spin-glass transition as seen experimentally since a consensus is now developing that the d = 3 Ising model does have a spin-glass phase transition at non-zero temperatures [11, 31] (the Ising model can be considered to be a Heisenberg model with strong uniaxial anisotropy). The results of this work show that anisotropy (in this case RMA) may actually induce double-transition behavior and we believe that these results implicate anisotropy as a cause of double-transition behavior in the transition metal and Gd systems discussed above. We speculate that when exchange fluctuations are present only an exceedingly small aniso-

tropy (smaller than that in the Er system of this work) is required to produce double-transition behavior.

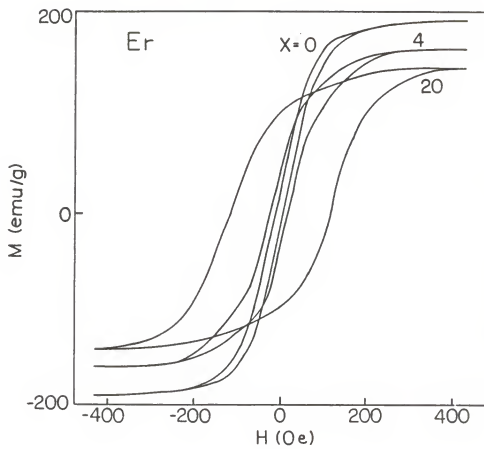


Fig. 5.5 Hysteresis loops at 4.2 K in the Er system.

CHAPTER 6

SCALING AT THE SPERMAGNETIC TRANSITION

A SM state can be induced by alloying Gd-Co with anisotropic rare-earths as discussed in chapter 4. A non-linear scaling of the magnetic isotherms is expected to hold at this transition similar to that at the SG transition (where exchange fluctuations are important) if the transition is a true phase transition rather than a gradual freezing of the spins [32]. Othman [4] studied the scaling behavior of non-linear susceptibility for $R = Tb$ and $x = 4, 10$ and 30 at. % alloys to determine whether the SM transition is a true phase transition. A good scaling of the isotherms was not obtained. Here we study the scaling behavior for the $x = 50$ at. % Tb alloy by measuring non-linear magnetization in a vibrating sample magnetometer (VSM). We use the VSM instead of ac susceptibility because high fields (up to 80 kOe) and good temperature control (0.05 - 0.1 % in VSM compared to 0.5 % error in ac susceptibility) are available. High field measurements were made (up to 80 kOe) using a superconducting magnet and low field (0 - 1000 Oe) measurements were made using a wire wound coil.

Most of the work in this Chapter has been reported in ref. [32]. In the Tb alloy we show that the magnetic isotherms follow a non-linear scaling below 700 Oe. Above 1 kOe we find the rather surprising result that the magnetic isotherms obey linear scaling expected for a FM transition.

We describe these results in the following sections.

6.1 Linear Scaling

A ferromagnetic phase transition may be characterized by the power law behavior of various magnetic quantities close to the transition. This is usually done via the power law critical exponents. Critical exponents α , β , γ , δ are defined by;

$$\begin{aligned}C_H &= t^{-\alpha} \\ M &= (-t)^\beta \\ \chi &= t^{-\gamma} \\ M &= H^{1/\delta}\end{aligned}\tag{6.1}$$

where C_H , M , χ , H are specific heat at constant magnetic field, magnetization, susceptibility, magnetic field respectively and $t = (T-T_C)/T_C$. It can be shown via the scaling hypothesis [33] for continuous phase transitions that there are only two independent critical exponents. If β and δ are measured, α and γ may be obtained using

$$\begin{aligned}\alpha &= 2 - \beta(\delta + 1) \\ \gamma &= \beta(\delta - 1).\end{aligned}\tag{6.2}$$

The scaling hypothesis may also be used to rewrite the ferromagnetic equation of state in the form [34]:

$$m = f_{\pm}(h)\tag{6.3}$$

where

$$m = M/t^\beta, \quad h = H/t^{\beta\delta}.$$

The + and - signs correspond to two branches of the equation

of state with $T > T_c$ and $T < T_c$ respectively. This equation of state indicates that all the magnetic isotherms for $T > T_c$ should collapse onto one branch (+) and all the magnetic isotherms for $T < T_c$ should collapse onto another branch (-) when plotted in the reduced units m and h .

Neither the form of the function f or the critical exponent values are predicted by the scaling hypothesis. Fig. 6.1 shows the magnetization data (reduced units) as a function of applied field in linear and logarithmic form to resolve the scaling at both high and lower fields. The exponents β and δ were determined by varying them on a grid with $0.2 < \beta < 0.8$ and $2.0 < \delta < 7.0$. These limits encompass all values of β and δ found previously ($0.32 < \beta < 0.55$ and $3.5 < \delta < 5.5$). Good scaling is obtained with a collapse of the magnetization isotherms onto two separate curves with the exponents β and δ of 0.45 ± 0.01 and 4.0 ± 0.1 respectively. These values are close to those found in a number of other metallic glasses and to the Heisenberg $d = 3$ model [34]. Below about 1 kOe large deviations from scaling become apparent as may be seen from Fig. 6.2 where data from 80 kOe down to 50 Oe are plotted. This should be contrasted with a number of ferromagnetic systems where good scaling is found down 50 Oe and below with the low field limit being determined by demagnetization field effects [20, 34].

6.2 Non-linear Scaling

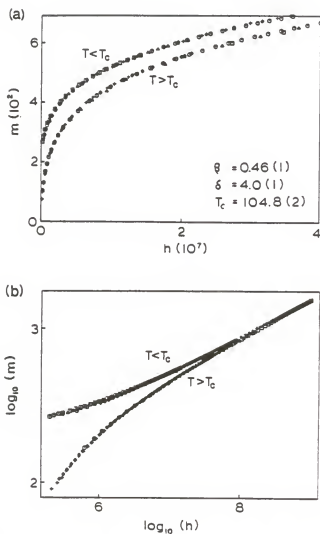


Fig. 6.1 Scaling of the magnetic isotherms for the $x = 50$ at. % Tb alloy plotted in (a) linear and (b) logarithmic form. The temperatures of the magnetic isotherms are $(T)T_c$: 111.3 (+), 109.8 (\diamond), 108.4 (\circ), 106.8 (Δ), 105.4 (\square), $(T)T_c$: 104.1 (+), 102.4 (\diamond), 101.0 (\circ), 99.7 (Δ), 98.5 (\square)

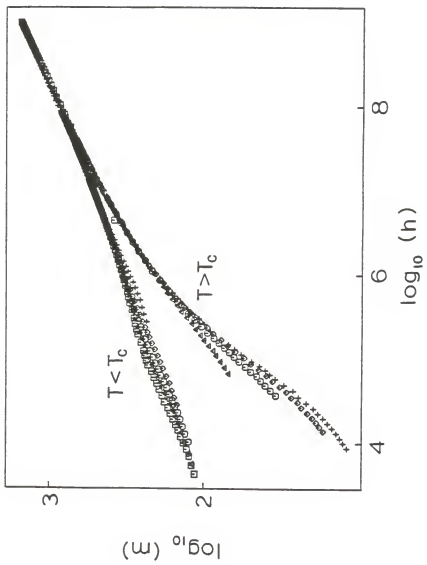


Fig. 6.2 Deviations from linear scaling below about 1 kDe.

The data up to 80 kOe was tested to see how well they follow a non-linear scaling equation of state. Magnetic isotherms below 700 Oe were taken using a wire wound coil to avoid hysteresis and remanent field effects (about 20 Oe) in the magnetic field of the superconducting magnet.

The transition can be described by the power law exponents α' , β' , γ' , δ' defined by;

$$\begin{aligned} C_H &= t^{-\alpha'} & (6.4) \\ M &= (-t)^{\beta'} \\ \chi &= t^{-\gamma'} \\ M &= H^{1/\delta'} \end{aligned}$$

where C_H , M , χ , H are specific heat at constant magnetic field, magnetization, susceptibility, magnetic field respectively, $t = (T - T_C)/T_C$. According to the scaling hypothesis for continuous phase transitions there are only two independent static critical exponents. If, for example, β' and γ' are measured, α' and δ' may be determined from the equalities;

$$\begin{aligned} \alpha' &= 2 - \beta'(\delta' + 1) & (6.5) \\ \delta' &= (\beta' + \gamma')/\beta'. \end{aligned}$$

According to the scaling hypothesis the general magnetic equation of state $M = M(t, H)$ can be recast in the form [35, 36]

$$m_{n1} = f_{\pm}(h_{n1}) \quad (6.6)$$

where

$$m_{n1} = M_{n1} / t^{(3\beta' + \gamma')/2}$$

$$h_{nl} = H / t^{(\beta' + \gamma')} .$$

$M_{nl} = \chi_0(T)H - M(H, T)$ is the non-linear magnetization and $\chi_0(T)$ is the zero field susceptibility calculated from the initial slope of the isotherm for a given temperature. The + and - signs correspond to two branches of the equation of state with $T > T_C$ and $T < T_C$ respectively. In addition the branch corresponding to $T > T_C$ should have a high field slope of $2/S'$ and a low field slope of 2 on a log-log plot of the reduced variables m_{nl} and h . The exponents β' and γ' were varied on a grid with $0.5 < \beta' < 3$ and $1 < \gamma' < 8$. These limits encompass all previous measurements of β' and γ' well within their bounds as can be seen from Table 6.1. The best collapse of the non-linear magnetic isotherms corresponded to $\beta' = 1.30 \pm 0.05$ and $\gamma' = 3.8 \pm 0.2$ as shown in Fig. 6.3. It was found that the non-linear scaling worked, i.e. the isotherms collapse onto two separate curves, for fields < 700 Oe and only these results are plotted. For fields > 700 Oe non-linear scaling did not work. These values are compared to β' and γ' values for other RMA systems and also some SG systems in Table 6.1. At low reduced fields the slope of the lower curve in the logarithmic plot of Fig. 6.3 is close to 2 as expected [36], but high enough reduced fields to obtain the limiting $2/S'$ (S' may be obtained from $S' = 1 + \gamma'/\beta'$) slope at high reduced fields have apparently not been achieved.

6.3 Discussions

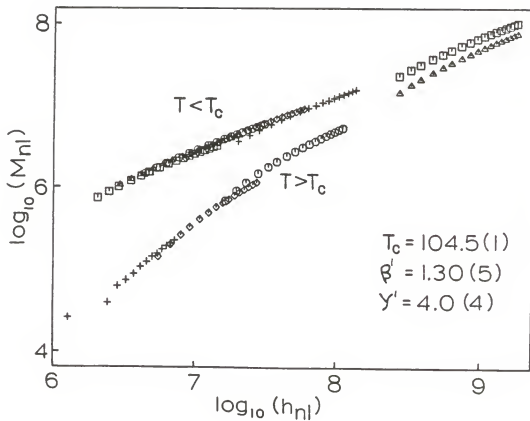


Fig. 6.3 Non-linear scaling of the magnetic isotherms for the $x = 50$ at. % Tb alloy plotted in logarithmic form. The temperatures of the magnetic isotherms are ($T > T_c$): 108.5 (\square), 107.5 (Δ), 106.4 (\circ), 105.3 (\diamond), ($T < T_c$): 104.3 (\square), 103.2 (Δ), 101.8 (\circ), 100.5 (\diamond)

System		ρ'	γ'	δ'	H range (Oe)	t range	Ref.
Small Anisotropy and Large Exchange Fluctu- ations	CsNiFeF ₆	1.2±0.1	3.0±0.5	3.5±0.5	0-100	0.01-0.05	[39]
	AlMnSi	1.4±0.1	3.4±0.1	3.4±0.1	0.01-20	0.08-0.4	[39]
	CuMn(4.6%Mn)	1.1±0.2	3.4±0.4	4.2±0.1	4-400	0.01-0.9	[40]
	AgMn (0.4-20% Mn)	1.0±0.1	2.2±0.2	0.1±0.2	10-400	0.01-0.1	[41]
Large	AuFe(1.5%Fe)	0.9	1.1±0.2	2.0±0.2	10-100	0.001-0.1	[42]
	DyNi _{1.33}	1.22±0.1	2.0±0.1	2.7±0.1	2.4-100	0.005-0.25	[37]
Anisotropy	Tb ₆₄ Fe ₂₀₆ a ₁₆	1.7±0.1	3.7±0.1	3.2±0.1	40-288	0.002-0.13	[43]
	Gd ₁₅ Tb ₅₀ Co ₃₅	1.3±0.05	3.8±0.2	3.8±0.2	100-900	0.005-0.04	This work

Table 6.1 Non-linear exponents in SG and SM systems.

We believe that although the RMA in this system is strong, the strong exchange allows the system to cross-over to standard ferromagnetic behavior in a sufficiently large field (Tb, of all the rare-earth alloys, decreases the exchange strength the least). In order to see the non-linear critical phenomena characteristic of the ground state of this system, fields below about 700 Oe must be used to avoid strongly perturbing the speromagnetic ground state. It is not surprising that large fields () 1 kOe) produce a FM-like state by lining up the spins but it is surprising that the magnetic isotherms follow critical behavior for a FM transition.

It has been suggested that systems following non-linear scaling behavior fall into two main types [37] and the low values of γ' and δ' in DyNi_{1,33} and AuFe alloys [Table 6.1] compared to SG systems without anisotropy have been used as evidence in favor of this hypothesis. The exponents of this work and of Tb₆₄Fe₂₀Ga₁₆ reported in ref. [43] do not follow this pattern as may be seen from Table 6.1. It is likely that different classes of non-linear scaling systems (implying different critical exponents) do exist but we do not believe any evidence exists in the measured critical exponents so far for a classification which separates SM (strong anisotropy) and SG (weak anisotropy and strong exchange) systems.

CHAPTER 7

SUMMARY AND CONCLUSIONS

We have studied ac susceptibility and dc magnetization of metallic glasses with composition $Gd_{65-x}R_xCo_{35}$, where rare-earth R represents La, Ce, Pr, Nd, Sm, Tb, Dy, Ho, Er. Alloying with La or Ce which are both non-magnetic in our system leads to a gradual reduction in the PM-FM transition temperature of $Gd_{65}Co_{35}$ due to the decrease in average exchange. Alloying with all of the anisotropic rare-earths except Er introduces a strong RMA and leads to a cross-over from PM-FM to PM-SM transition behavior. The Er system shows double-transition behavior for $1 < x < 8$ at. %, that is a sequence of PM to FM to SM transitions with decreasing temperature. At about $x = 8$ at. % the double-transition behavior is replaced by a single PM-SM transition. The Er samples have the smallest RMA strength for a given composition of all the anisotropic rare-earths studied. We conclude that the double-transition behavior in the Er system is due to the small RMA present in this system.

The linear and non-linear magnetization were studied in the Tb system with $x = 50$ at. %. We find that the magnetization isotherms follow a non-linear scaling for $H < 700$ Oe much like that found in SG systems. These results show that in the limit of low fields the PM-SM transition acts as a phase transition in its scaling behavior and is similar to that found for a PM-SG transition. We also find

that large enough fields (1 kOe) induce a FM state with the magnetic isotherms following the standard FM scaling equation of state.

REFERENCES

- [1] A. I. Gubanov, *Fiz. Tver. Tela* 2, 502 (1960).
- [2] J. J. Rhyne, S. I. Pickart and N. A. Alperin, *Phys. Rev. Lett.* 29, 1562 (1972).
- [3] R. Harris, M. Plischke and M. J. Zuckermann, *Phys. Rev. Lett.* 31, 160 (1973).
- [4] F. Othman, Master Thesis, Kansas State University (1985).
- [5] M. A. Ruderman and C. Kittel, *Phys. Rev.* 96, 95 (1954)
T. Kasuya, *Prog. Theor. Phys.* 16, 45 (1956)
K. Yosida, *Phys. Rev.* 106, 893 (1957).
- [6] *Amorphous Magnetism* by Takahito Kaneyoshi, CRC Press, Boca Raton, Florida (1984).
- [7] D. J. Sellmyer and S. Nafis, *J. Appl. Phys.* 57(1), 3584 (1985).
- [8] M. Gabay and G. Toulouse, *Phys. Rev. Lett.* 47, 201 (1981).
- [9] Y. Yeshurun, M. B. Salamon, and K. V. Rao, *Phys. Rev. Lett.* 45, 1366 (1980).
- [10] G. Dublon and Y. Yeshurun, *Phys. Rev.* B25, 4899 (1982).
- [11] A. T. Ogielski and I. Morgenstern, *Phys. Rev. Lett.* 54, 928 (1985)
A. T. Ogielski and I. Morgenstern, *J. Appl. Phys.* 57, 3382 (1985).
- [12] R. A. Pelcovits, E. Pytte, and J. Rudnick, *Phys. Rev.*

- Lett. 40, 476 (1978).
- [13] E.M. Chudnovsky, W.M. Saslow, and R.A. Serota, Phys. Rev. B33, 251 (1986).
- [14] K. Fukamichi, T. Goto, T. Sakakibara, S. Todo, K. Aoki, and T. Masumoto, J. Magn. Magn. Mater. 54, 239 (1986).
- [15] Intro. to Solid State Physics, Kittel.
- [16] Handbook on the Physics and Chemistry of Rare Earths by M.B. Maple, L.E. DeLong, and B.C. Sales, North Holland Press, Amsterdam (1979).
- [17] J.J. Rhyne, J.A. Schelling, and N.C. Koon, Phys. Rev. B10, 4672 (1974).
- [18] M.J. O'Shea, K.M. Lee, and F. Othman, Phys. Rev. B34, 4944 (1986).
- [19] A. Berton, J. Chaussy, J. Odin, R. Rammal, J. Souletie, J.L. Tholence, R. Tournier, F. Holtzberg, and S. Von Molnar, J. Appl. Phys. 52, 1763 (1981).
- [20] M.J. O'Shea and D.J. Sellmyer, Phys. Rev. B32, 7502 (1985).
- [21] R.B. Goldfarb, K.V. Rao and H.S. Chen, Sol. St. Comm. 54, 799 (1985).
- [22] G. Hadjipanayis, D.J. Sellmyer, and B. Brandt, Phys. Rev. B32, 3349 (1982).
- [23] E. Callen, Y.J. Liu, and J.R. Cullen, Phys. Rev. B16, 263 (1977).
- [24] B.R. Coles, B.V.B. Sarkissian, and R.H. Taylor, Phil.

- Mag. B37, 489 (1978).
- [25] Y. Yeshurun, M.B. Salamon, K.V. Rao, and H.S. Chen, Phys. Rev. B24, 1536 (1981).
- [26] M.A. Manheimer, S.M. Bhagat, and H.S. Chen, J. Magn. Mag. Mat. 38, 147 (1983).
- [27] I.A. Campbell, H. Hurdequint, and F. Hippert, Phys. Rev. B33, 3540 (1986).
- [28] J.R. Banavar and M. Cieplak, Phys. Rev. Lett. 48, 832 (1982).
- [29] W.L. McMillan, Phys. Rev. B31, 342 (1985).
- [30] A. Chakrabarti and C. Dasgupta, Phys. Rev. Lett. 56, 1404 (1986).
- [31] R.N. Bhatt and A.P. Young, Phys. Rev. Lett. 54, 924 (1985); A.P. Young, J. Appl. Phys. 57, 3361 (1985).
- [32] M.J. O'Shea, K.M. Lee, and D.J. Sellmyer, to be published in J. Appl. Phys., April 1987.
- [33] Intro. to Phase Transitions and Critical Phenomena by Eugene Stanley, Oxford University Press, London (1971).
- [34] S.N. Kaul, J. Magn. Magn. Mat. 53, 5 (1985).
- [35] J. Chalupa, Sol. State Comm. 24, 429 (1977).
- [36] J. Phys. Lett. (Paris) 45, L-665 (1984).
- [37] B. Dieny and B. Barbara, Phys. Rev. Lett. 57, 1169 (1986).
- [38] C. Pappa, J. Hammann, and C. Jacoboni, J. Phys. (Paris) 46, 637 (1985).

- [39] P. Beauvillain, C. Chappert, J.P. Renard, and J. Seiden, *J. Magn. Magn. Mat.* 54-57, 127 (1986).
- [40] B. Barbara, A.P. Malozemoff, and Y. Imry, *Phys. Rev. Lett.* 47, 1852 (1981).
- [41] H. Bouchiat, *J. Phys. (Paris)* 47, 71 (1986).
- [42] T. Taniguchi, H. Matsuyama, S. Chikazawa, and Y. Miyako, *J. Phys. Soc. Japan* 52, 4323 (1983).
- [43] D.J. Sellmyer and S. Nafis, *Phys. Rev. Lett.* 57, 1173 (1986).

MAGNETIC PHASE TRANSITIONS
IN RARE-EARTH-RICH GLASSES

by

KWAN MYUNG LEE

B.S., Busan National University, KOREA, 1982

AN ABSTRACT OF A MASTER'S THESIS

Submitted in partial fulfillment of the
requirements for the degree

MASTER OF SCIENCE

Department of Physics

KANSAS STATE UNIVERSITY
Manhattan, Kansas

1987

ABSTRACT

We have studied ac susceptibility and dc magnetization of metallic glasses with compositions $Gd_{65-x}R_xCo_{35}$, where R represents the rare-earths La, Ce, Pr, Nd, Sm, Tb, Dy, Ho, Er. Alloying $Gd_{65}Co_{35}$ with anisotropic rare-earths induces a random magnetic anisotropy and leads to a cross-over from paramagnetic-ferromagnetic to paramagnetic-speromagnetic transition behavior. The Er systems show different behavior with double-transition behavior for $1 < x < 8$ at. %. We argue that this is due to the small anisotropy in Er alloys and this result indicates that anisotropy can produce double-transition behavior. We have studied the linear and non-linear magnetization in the Tb system with $x = 50$ at. %. We show that for large enough magnetic fields the system shows standard ferromagnetic scaling but for low enough fields the system crosses over to a behavior describable by non-linear scaling. This latter result is consistent with the PM-SM transition being a true phase transition.